Research Article

Bittern-Derived Mg/Al Layered Double Hydroxide Adsorbent for Potential Ciprofloxacin Removal in Water Treatment Application

Swasmi Purwajanti*
Research Center for Electronics, National Research and Innovation Agency (BRIN), Bandung, Indonesia

Ratih Amalia
Nano Center Indonesia, Jalan Raya PUSPIPTEK, South Tangerang, Banten, Indonesia

Selvi Astuti Listyani
Faculty of Mathematics and Science, Garut University, Jawa Barat, Indonesia

Fitri Dara, Akmal Zulfi M and Muhamad Nasir
Research Center for Environmental Technology and Clean Technology, National Research and Innovation Agency (BRIN), South Tangerang, Banten, Indonesia

Athanasia Amanda Septevani
Research Center for Electronics, National Research and Innovation Agency (BRIN), Bandung, Indonesia

Alfian Noviyanto
Nano Center Indonesia, Jalan Raya PUSPIPTEK, South Tangerang, Banten, Indonesia
Department of Mechanical Engineering, Mercu Buana University, Jakarta, Indonesia

* Corresponding author. E-mail: swas002@brin.go.id DOI: 10.14416/j.asep.2026.02.001
Received: 2 September 2025; Revised: 28 October 2025; Accepted: 26 November 2025; Published online: 3 February 2026

Abstract
The presence of ciprofloxacin (CIP), an antibiotic, in pharmaceutical wastewater has emerged as a significant environmental concern. This study presents the synthesis of magnesium/aluminum layered double hydroxide (MAL) through a co-precipitation method, utilizing seawater bittern as the magnesium source, with the objective of addressing CIP removal effectively. MAL was prepared at three different pH levels (5, 9, and 12), resulting in three distinct samples: MAL5, MAL9, and MAL12. Among these, MAL9 was identified as the most effective variant, exhibiting well-formed crystal structures alongside the highest adsorption capacity for CIP, achieving a removal rate of 63%. Moreover, we evaluated several factors that influence the adsorption process, including the dosage of the adsorbent, the solution's pH, and the presence of co-ions. The findings indicated that optimal adsorption occurs at a concentration of 1 mg/mL within a pH range of 6 to 9, demonstrating significant resistance to both monovalent and divalent co-ions. The adsorption mechanism was further investigated through isothermal modeling (the Freundlich isothermal model), resulting in data that aligned with the Freundlich isothermal model, which indicated a maximum adsorption capacity of 95.15 mg/g at the concentration of CIP of 100 mg/L. Kinetic analysis showed that the sorption process follows a pseudo-second-order model, reaching equilibrium in about 100 minutes. The MAL demonstrated an impressive reusability, maintaining 90% to 50% performance over three adsorption-desorption cycles. Thus, bittern-derived MAL is an effective adsorbent for CIP removal and promotes the sustainable use of bittern waste as a magnesium precursor in functional nanomaterials synthesis.

Keywords: Adsorption, Bittern, Ciprofloxacin, Layered double hydroxides, Water treatment

1 Introduction

Water pollution has emerged as a critical global issue, significantly impeding access to clean water and proper sanitation, as emphasized in the United Nations Sustainable Development Goal 6 [1]. One of the most troubling contributors to water pollution is the presence of pharmaceuticals and medical waste, particularly antibiotics, which are among the most commonly consumed medications. Ciprofloxacin (CIP), a second-generation fluoroquinolone, stands out as the most frequently prescribed antibiotic due to its broad-spectrum efficacy against a range of Gram-negative and some Gram-positive bacteria [2]. The therapeutic effectiveness of CIP lies in its ability to inhibit bacterial cellular replication, thus limiting their proliferation [3]. While this property is beneficial in medical applications, the extensive prescription of CIP, coupled with incomplete metabolic processing [4], has resulted in significant concentrations of the drug in municipal water systems—reportedly reaching up to 20,000 ng/L [5]. This situation raises environmental concerns and highlights the pressing need to address antibiotic pollution. The health implications associated with antibiotic contamination are substantial; elevated doses of CIP can lead to severe conditions such as thrombocytopenia, acute renal failure, eosinophilia, increased liver enzymes, and leucopenia [6]. Moreover, exposure to even low concentrations of antibiotics poses a risk for the development of resistance and genetic transfer among both human and animal populations [7]. Thus, addressing the removal of ciprofloxacin waste has become an urgent priority.

Notably, CIP exhibits remarkable resistance, not only to biodegradation [8] but also to pH changes. CIP exhibits persistent performance across a range of pH levels in water. It exists as CIP^{+} at low pH due to the activation of the NH_2^{+} group, transitioning to a zwitterionic form ($CIP^{+/-}$) between pH 3 and 9, and appears as CIP^{-} at higher pH levels as a result of the negative charge from hydroxyl groups [9], [10].

The conventional techniques employed for treating wastewater are often inadequate for addressing contaminants of emerging concern (CIP pollutants) due to their resistance to biodegradation [8]. Therefore, a variety of advanced treatment methods have been evaluated, including catalytic [11], photocatalytic, and ozone-based oxidation [12], as well as biological treatment and reverse osmosis [2], [13]. Their high cost and complex treatment are major obstacles. However, these advanced methodologies can be prohibitively expensive and necessitate extensive maintenance. In the process to compromise the efficiency and economical approach, the attention has shifted to the adsorption process. A more practical solution lies in the adsorption process, which is based on the principles of mass transfer and the availability of surface sites. This process utilizes adhesion forces that surpass cohesive forces, thereby attracting molecules to the surface of the adsorbent material [2], [14]. Several critical factors influence the efficiency of adsorption, including surface area, concentration of the adsorbate, pH level of the solution, and duration of contact. The mechanisms underlying adsorption have been extensively researched to elucidate the interactions between the adsorbate and the adsorbent through various theoretical models, such as Henry's law [15], Harkin-Jura model [16], and isothermal Langmuir and Freundlich equations [17], [18]. Additionally, characteristics such as surface area, porosity, and heterogeneity can be effectively assessed. Upon establishment of the adsorption process, the behavior of sorption can be robustly predicted using a kinetic approach. Typically, the adsorption process adheres to a pseudo-kinetic order, which accurately describes the influence of physical and chemical processes governing sorption [10], [13], [14].

Layered double hydroxides (LDH) represent a significant category of ionic lamellar solids, consisting of metallic ions and interlayer anions. These materials are characterized by the general formula $[M_{1-x}^{2+}M_x^{3+}(OH)_2(A^{n-})_{x/n}]^{x+}.mH_2O$ [19]. The designation of M^{2+} and M^{3+} is the combination of metallic ions that originate from Mg^{2+}, Co^{2+}, Ni^{2+}, Zn^{2+}, and Cu^{2+} as divalent ions, and (e.g., Al^{3+}, Fe^{3+}, Ga^{3+} as trivalent ions, ranging from 2-5 as a molar ratio of M^{2+}/M^{3+} [20], [21]. LDH exhibits a distinctive brucite-like structure featuring two layers of crystallized hydroxide, imparting a positive net charge to its surface [22], [23]. The fundamental characteristics of LDH comprise regular basal spacing that supports its crystalline phase, an interlayer region that accommodates anions, and a brucite framework formed from hydroxylated metallic ions [24]. The adsorption process involves the interaction between adsorbate molecules and metallic ions within the brucite framework, leading to a charge-balancing effect facilitated by existing anions in the interlayer regions [24]. The affinity of the brucite framework is critical for adsorbate interactions, which underscores

the importance of studying various combinations of metallic ions. Among these, the pairing of magnesium (M^{2+}) with aluminum (M^{3+}) has been extensively researched and frequently serves as the foundation for further modifications of LDHs [25]–[27], such as MgFeAl-, MgCuAl-, and MgZnAl-LDHs, which possess diverse properties, including photocatalytic, optical, and flame-retardant features [28]. LDH-based adsorbents have been studied for antibiotic adsorbent. Previous studies have been carried out to adsorb antibiotics using layered bimetallic hydroxides such as Mg/Fe LDHs. Qiu *et al.*, prepared Mg/Fe LDHs at a molar ratio of 5:1 and investigated their adsorption performance to remove low concentrations of Norfloxacin with an adsorption capacity of 97.07 mg/g at neutral pH. Also, De Lima *et al.*, prepared Mg/Fe LDH for amoxicillin adsorption in water and reached the adsorptive capacity of 9.11 mg/g. Ni/Fe LDH was also synthesized by dos Santos *et al.*, to remove sulfadiazine with a maximum adsorption capacity of 631.5 mg/g. These studies underline the importance of LDH-based material in emerging pollutants removal, especially antibiotics, as the cations and anions present in the structure of LDH may intercalate the antibiotic molecules in the interlayer region through ion exchange with the original anion.

While the synthesis of LDH systems from different metallic sources is well-documented, it predominantly relies on commercial reagents. Therefore, expanding the sources of magnesium for LDH synthesis, especially utilizing readily available by–products, is highly desirable.

Bittern, a by-product of salt production, emerges as a rich alternative source of Mg^{2+}. Indonesia stands as the largest global producer of bittern, which is abundant in various minerals and salts, including sodium, potassium, sulfate, chloride, and magnesium. The concentration of magnesium in bittern can reach levels as high as 60 g/L, with Mg^{2+} content exceeding 20 g/L. Many studies have been carried out to lock out the potency of bittern as Mg^{2+} precursor for synthesizing Magnesium-based nanomaterial, for examples MgO and $Mg(OH)_2$ nanoparticles, which have wide applications such as sensors, catalyst supports, photonic devices, electro-optical devices and bactericides because of their good surface reactivity. The preparation techniques involve precipitation, decarboxylation/precipitation, sonochemical process and electrochemical method, which are considered as facile and environmentally–friendly. Moreover, these nanomaterial preparation methods are proven to be convenient to be up-scaled for practical application industry. The utilisation of bittern, which is considered as waste as Mg^{2+} precursor, could realize the concept of zero waste and give the added-value of bittern itself as a precursor of functional nanomaterials.

This study aims to synthesize Mg/Al layered double hydroxides (MAL) for applications in water treatment, specifically targeting the removal of ciprofloxacin (CIP). We propose a thorough investigation into the structural properties and adsorption performance utilizing magnesium sourced from bittern, an approach that has not been previously reported. By addressing the challenge of CIP as a pollutant through adsorption using the abundant by-product of bittern, we present a comprehensive solution that effectively tackles both environmental concerns of water treatment and waste management. To this end, we collected bittern from the saltpond in Pamekasan-Madura Island, Indonesia, and subsequently filtered it to remove impurities. The Mg^{2+} precursor derived from bittern was combined with $AlCl_3.6H_2O$ as the Al^{3+} source. The synthesized Mg/Al-LDHMAL was characterized thoroughly using X-ray diffraction (XRD), scanning electron microscope (SEM), and Fourier transform infrared (FTIR). Additionally, to assess the surface area available for adsorption, we measured the surface area. We initiated our investigation of adsorption performance by considering various influential factors, including the pH of the synthesis process, the dosage of the adsorbent, the pH of the adsorbate, and the presence of co-ions. The maximum adsorption capacity was evaluated using an isothermal adsorption model, while the kinetic order analysis was employed to elucidate the dynamics of the sorption process. Finally, we demonstrated the potential for reusability of this material by conducting adsorption–desorption tests over multiple cycles.

2 Experimental Section

2.1 *Materials*

Commercial materials were of an analytical grade and directly used without further purification. Ciprofloxacin, sodium hydroxide (NaOH), aluminum chloride hexahydrate ($AlCl_3.6H_2O$), and sodium bicarbonate (Na_2CO_3) were procured from Sigma-Aldrich Co. (USA). A stock solution of ciprofloxacin of 50 mg L^{-1} was prepared and diluted using Ultrapure

Milli-Q water. Solution pH was adjusted using 0.1 N HCl and 0.1 N NaOH. Bittern was supplied from a salt pond in Pamekasan-Madura Island, Indonesia, with the concentration of magnesium, sulphate, chloride, sodium, and calcium of 58,000 mg/L, 96,608 mg/L, 15.05%, 2.54% and 0.01%, respectively. It is worth noting that ionic concentrations in bittern may vary over different origins, varying from the sea to the ocean and are also influenced by seasons.

2.2 *Synthesis of MAL*

The synthesis of MAL was achieved through a co–precipitation method at a designated pH level. The magnesium source, Mg^{2+}, was derived from a filtered bittern solution, which contained 58,000 mg/L of magnesium. The concentration of magnesium was determined using an inductively coupled plasma optical emission spectrometer (ICP-OES) and adjusted to establish the targeted molar ratio of metal ions, specifically maintaining an M^{2+}/M^{3+} ratio of 3. The aluminum component, Al^{3+}, was sourced from $AlCl_3 \cdot 6H_2O$, facilitating the formation of the MAL. The balancing anions were introduced through a combination of sodium hydroxide (NaOH) and sodium carbonate (Na_2CO_3). The preparation protocol commenced with the addition of 50 mL of $AlCl_3 \cdot 6H_2O$ mixed with 50 mL of the filtered bittern solution, ensuring the establishment of a M^{2+}/M^{3+} molar ratio of 3.0/1.0. Subsequently, anionic solutions were prepared by combining 50 mL of 0.4 mol L^{-1} Na_2CO_3 with 50 mL of 1.5 mol/L NaOH. This anionic solution was gradually introduced to the previously prepared metal solution while carefully maintaining pH levels of 5, 9, and 12, corresponding to the designations MAL5, MAL9, and MAL12, respectively. The precipitation process was conducted in a boiling flask, placed in a water bath maintained at a temperature of 80 °C for approximately six hours. The resultant precipitates were subjected to filtration and washing to achieve a neutral state, followed by a drying phase at 70 °C for a duration of 12 to 24 h, culminating in the formation of the MAL system.

2.3 *Characterization*

XRD analysis was conducted utilizing the Bruker D8 Advance 3kW instrument equipped with a Cu-Kα source at 40 kV, covering a 2θ angle range of 10°−90°. The surface morphology of the samples was characterized through SEM using the Hitachi SU–3500 microscope, with magnifications of 2,500 times and 10,000 times at 20 kV. The functional groups present in the material were evaluated using FTIR spectroscopy, employing the Thermo Scientific Nicolet iS–10 across a range of wave numbers from 400 to 4000 cm^{-1}. Additionally, specific surface area measurements and pore size analyses were performed using the Brunauer–Emmett–Teller (BET) and Barrett–Joyner–Halenda (BJH) methods, respectively, employing the Quantachrome Nova 4200e Gas Sorption Instrument with accuracy within 1–3%.

2.4 *Adsorption experiments*

A static adsorption test was conducted under room temperature conditions with magnetic stirring at a speed of 200 rpm for a duration of 4 h to facilitate equilibrium. A 50 mL conical flask was utilized, containing the synthesized adsorbent at a loading concentration of 1 mg/mL, with an initial CIP concentration of 50 mg/L, which was selected as the model contaminant to investigate the adsorption properties of the Mg/Al LDH.

The influence of foreign anions on the adsorption capacity of CIP was also examined. Specifically, anions such as Cl^-, CO_3^{2-}, SO_4^{2-}, and PO_4^{3-} were chosen as interfering substances for the adsorption experiments, each at a concentration of 1 mol/L. Additionally, the effects of solution pH and adsorbent dosage on the adsorption of the antibiotic were analyzed.

The potential for regenerating the MAL 9 after CIP adsorption was also explored. After the adsorption process, the adsorbent was regenerated through a washing procedure using acetic acid at pH 3, followed by separation via centrifugation and drying in an oven at 60 °C. This regeneration process was performed over four cycles, with an initial concentration of CIP in the regeneration solution of 50 mg/L at pH 7 with an adsorbent concentration of 1 mg/mL. Acetic acid pH 3 was used to break the bound CIP on the surface of MAL 9, as CIP can dissolve in an acidic medium and at the same time to preserve the structure of exhausted adsorbent MAL 9.

The variations in the adsorption process were assessed by analyzing the absorbance of the solution using an Agilent UV–Visible spectrophotometer at a wavelength of 278 nm. The measurements were carried out in triplicates and the CIP adsorption performance data presented in this study were the mean values of triplicate measurements. Further

calculations established a correlation between the absorbance values and the concentration of remaining CIP in the solution, thereby enabling the quantification of the adsorbed molecules. The removal efficiency and adsorption capacities of the prepared adsorbent were calculated using Equations (1) and (2), respectively.

$$q = \frac{(Co-Ce)V}{W} \quad (1)$$

The variable (q_e) represents the adsorption capacity of CIP (mg/g). The parameters (Co) and (Ce) denote the initial and equilibrium concentrations of CIP in the solution (mg/mL), respectively. Additionally, (V) refers to the volume of the CIP solution (mL), while (W) indicates the dry weight of the adsorbent in milligrams (mg).

Kinetic experiments were conducted at a pH 7, with samples collected at intervals from 0 to 20 h. The adsorption dynamics and sorption rates were analyzed using a pseudo–second order kinetic model, as represented by Equation (2).

$$\frac{t}{q} = \frac{1}{kqe^2} + \frac{1}{qe}t \quad (2)$$

Adsorption isotherm studies were conducted for initial concentrations ranging from 10 to 100 mg/L using a consistent adsorbent loading. The resulting data were analyzed and fitted to various adsorption isotherm models, specifically the Langmuir and the Freundlich models.

3 Results and Discussion

3.1 *Characterizations of MAL*

A series of XRD analyses was performed to comprehensively understand the crystal structure. The XRD patterns of synthesized MAL9 are depicted, showcasing a series of distinct peaks in the diffractogram at 11.56°, 23.39°, 34.86°, 39.28°, 46.68°, 60.93°, and 62.28°, which correspond to Miller indices (003), (006), (012), (015), (018), (110), and (113), as illustrated in Figure 1(a). These peaks are characteristic of MAL and are in agreement with the standards provided in JCPDS No. 22–700. Notably, the prominent peaks observed at 11.56° and 23.39° for (003) and (006), respectively, reflect basal peaks, indicating the successful formation of a lamellar hydrotalcite-like material. Additionally, the distinct separation of the crystal planes represented by peaks at Miller indices (110) and (113) suggests a high degree of regularity within the anion layers [29]. This evidence affirms that MAL9 can be effectively synthesized using bittern at pH 9. Utilizing Bragg's equation, the calculated basal spacing was determined to be 7.624 Å. Relevant literature indicates a lamellar thickness of 4.81 Å [30]; consequently, the derived value for the interlayer anion is 2.814 Å, which is consistent with findings from other studies [31]–[33].

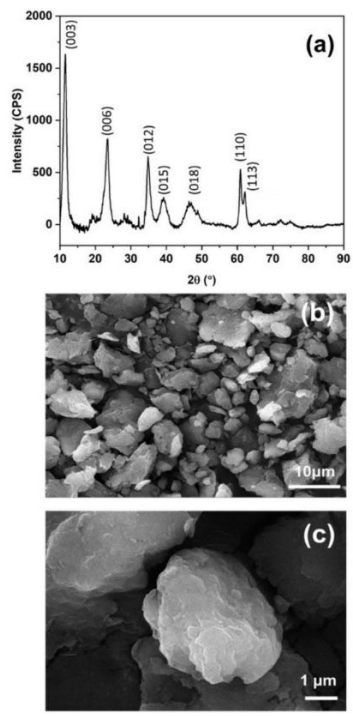

Figure 1: (a) XRD patterns and SEM images of a fractured surface of MAL9 in (b) 2500 and (c) 10,000 magnifications.

Table 1: Textural properties, surface, and pore characteristics of MAL materials.

Sample	Multipoint BET				
	S_{BET} (m^2/g)	D_p (nm)	VT (cm3/g)	c	r
MAL5	1655.00	1.81	1.50	2.50	0.99
MAL9	2671.00	1.82	2.43	2.43	0.99
MAL12	1326.56	1.95	1.29	1.29	0.99
Sample	**BJH Adsorption**				
	S_{BJH} (m^2/g)	V_{BJH} (cm^3/g)	D_{BJH} (nm)	%S meso	
MAL5	961.90	1.45	1.54	58.12	
MAL9	1566.00	2.38	1.53	58.63	
MAL12	813.22	1.25	1.53	61.30	

The morphology of the synthesized MAL sample was examined using SEM, as illustrated in Figure 1(b) and (c). Figure 1(b) reveals that the synthesized material exhibits a flattened morphology characterized by several granular fractions. The measured particle size is approximately 5 μm, which is consistent with findings from various studies on conventional precipitation processes, where particle sizes typically range from 1 to 10 μm [34], [35]. The gradual introduction of precursors during co-precipitation facilitates a thorough reaction, favoring the maximization of crystal growth stages over the rapid hot injection method employed in heat treatment processes. At higher magnifications, Figure 1(c) presents a distinct plate–like morphology of the particles, which aligns with observations reported in other studies [24], [36], confirming the presence of a well-developed layered structure. This clearly defined morphology corresponds closely with the prominent peaks observed in the XRD pattern of the MALsystem shown in Figure 1(a), particularly with the high–intensity peaks denoting the lamellar structure, specifically (003) and (006) planes.

The adsorption-desorption isotherms of nitrogen (N_2) and the corresponding pore size distribution have been utilized to characterize the pore properties within the structures of MAL5, MAL9, and MAL12, as illustrated in Figure 2 and summarized in Table 1. Notably, MAL9 exhibits the highest specific surface area (BET), whereas MAL12 demonstrates the lowest surface area. A larger specific surface area typically enhances the exposure of active sites and consequently leads to an increased adsorption capacity. Furthermore, the pore distribution spans approximately 1 to 50 nm, indicating that the MAL system comprises both mesoporous and microporous materials, with MAL9 showing a greater tendency towards macroporous structures (diameter > 50 nm). This trend generally aligns with the material's larger pore volume [33]. Specifically, the total pore volume of MAL9 reaches a maximum of 2.43 cm^3/g, followed by MAL5 at 1.5 cm^3/g and MAL12 at 1.29 cm^3/g, as detailed in Table 1. This range significantly exceeds that of other LDH-based materials, which often have pore volumes below 0.5 cm^3/g [10], [13], [33], [37]. The increased pore volume in MAL9 is likely a contributing factor to its superior capability for achieving the highest level of CIP adsorption in the later discussion. This enhanced transport pathway to the internal voids facilitates improved adsorption performance [33].

The hysteresis associated with microporous characteristics exhibits a broad range of P/P_0, whereas mesoporous materials typically display a narrower range of loops. This distinction is illustrated in Figure 2(b), which presents the hysteresis of N_2 adsorption-desorption. The observed hysteresis is subtle and approaches a reversible nature. This behavior closely resembles the findings reported by Saghir *et al.* [38], which demonstrated a Co/Ni-based LDH isotherm pattern characterized by an even slope and high linearity, underscoring the predominance of microporous materials reflecting the type 1 classification. The remarkable similarity in the extremely high surface area (as measured by BET) further supports these findings, as detailed in Table 1. However, it is important to note that these observations cannot be wholly extrapolated to the MAL materials, as the reference material is not entirely representative of an optimal LDH and significant discrepancies in textural property values are evident [39].

To address the obscureness, we have incorporated the analysis of the observed hysteresis (Figure 2(b)) alongside the BJH measurements (Table 1) to calculate the percentage of surface area attributed to mesoporous characteristics (%Smeso). Interestingly, our results indicate that the MAL materials yield a %meso value of approximately 50% of the total pore volume. This result suggests that the porous characteristics of MAL materials encompass a combination of microporous, mesoporous, and possibly macroporous features, a conclusion that resonates with findings documented in other scholarly articles [10]. Furthermore, the nearly reversible hysteresis observed in CoAl-LDH, as reported by Gao *et al.*, [40], is attributed to the two–dimensional plate–like structure of LDH. Notably, it notes the well–defined hysteresis of the mesoporous types H2 and H4, which are commonly associated with three–dimensional structured LDH, such as flower-like hollow or sphere formations [40]. This is consistent with the structural properties of MAL, which also exhibits a plate–like morphology (as depicted in Figure 1(b)) and demonstrates similar hysteretic behavior in connection with its micro–and mesoporous characteristics.

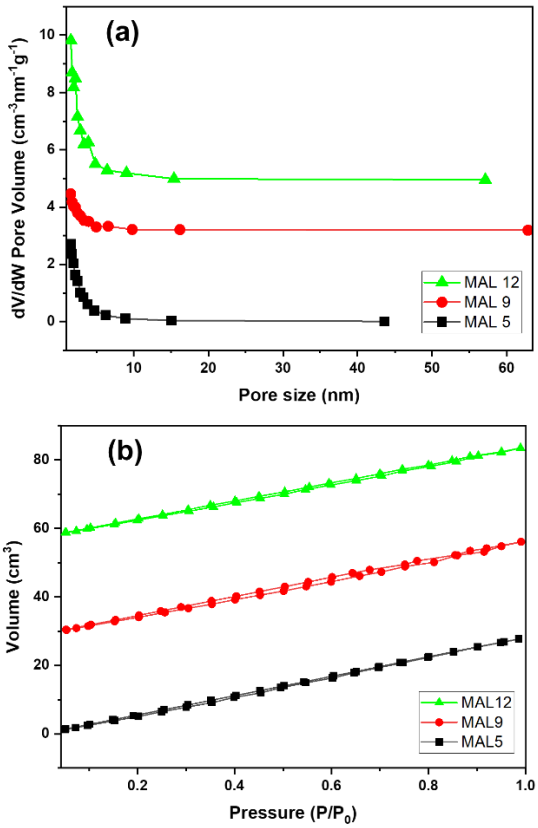

Figure 2: (a) N_2 adsorption and desorption isotherms, and (b) pore size distribution of MAL5, MAL9, and MAL12.

3.2 *Effect of pH in MAL synthesis*

The impact of pH on the synthesized MAL has been examined in detail. Co-precipitation is a well–established method utilized in the formation of various LDH–based materials. This process typically involves two key sequential steps: first, the transformation of the solution into one enriched with aluminum species, and second, the incorporation of divalent metal ions (such as Mg, Cu, or Zn) to achieve the hydrotalcite phase [41]. Numerous studies have investigated the mechanisms underlying LDH formation at a constant pH. However, the combinations of metals in the M^{2+}/M^{3+} ratio led to distinct optimal LDH formations across varying pH ranges. Specifically, the hydrotalcite phase of ZnAl-LDH displays a suboptimal crystalline structure at pH levels below 8, with the optimal crystallization occurring within the pH range of 8 to 10 [42]. Beyond pH 10, the predominant phase shifts to that of ZnO [43], [44]. While ZnAl-LDH demonstrates a relatively wide range of pH conditions suitable for crystal formation, the hydrotalcite phase of CuAl-LDH is formed within a narrow specific range, specifically at pH 8 [45]. Notably, the pH range for the formation of hydrotalcite in the case of MAL is significantly higher than that for CuAl-LDH or ZnAl-LDH, occurring predominantly between pH 9 and 10 [45], [46]. The synthesis mechanism of MAL under varying pH conditions was elaborated upon by Seron and Delorme [46], who noted that the aluminum ion precipitates immediately into a solid phase upon the initial addition of the base solution. The concentration of Al^{3+} ions significantly decreases following the introduction of the $NaOH/Na_2CO_3$ solution, a phenomenon typically attributed to the early precipitation of trivalent ions forming hydroxides. As the base solution continues to be added, the sequential precipitation of Mg^{2+} occurs due to the diminishing presence of Al^{3+} in the solution, corroborated by observations from Seron and Delorme [46] regarding the notable decrease in Mg concentration following the depletion of Al^{3+} at elevated pH levels. These findings illustrate a clear sequential behavior in the synthesis process [45], [46].

The pronounced sharp peaks observed at Miller indices (003), (006), and (012) in Figure 3 highlight the advantageous stacking sequence of basal spacing, which serves as the foundational structure of LDH–based materials. These peaks are critical indicators for tracking the formation of MALin response to pH variations (Figure 3). Notably, the co–precipitation process yielded no characteristic peaks of MAL when the solution's acidity was adjusted to pH 5 (MAL5). This absence can be attributed to the instability of certain fractions of the trivalent cation, resulting from a charge imbalance at higher acid concentrations. Consequently, the M^{2+}/M^{3+} ratio was inadequate to attain the necessary proportions for crystal phase development. Furthermore, it is plausible that hydrotalcite may have formed in an amorphous phase during this process [45]. In contrast, distinct sharp peaks emerged at pH 9 (MAL9) and became increasingly pronounced at pH 12 (MAL12), reflecting a more substantial formation of ordered layers. This observation is consistent with existing literature, which indicates that sharper XRD peaks for MAL formation are typically seen at pH levels ranging from 8.5 to 13.2 [46]. However, a secondary phase of hydromagnesite ($Mg_2(CO_3)_4(OH)_2.5H_2O$) is present in sample MAL12. Literature suggests that this phenomenon can be attributed to the reaction of magnesium from bittern under extreme alkaline

conditions, which occurred in two–step reaction, as shown in Equations (3) and (4). Conversely, some studies propose that brucite decomposition may occur due to an insufficient balance of negative charge arising from the abundance of MgOH, which may lead to inadequate charge levels. This imbalance has the potential to compromise the basal spacing of LDH and promote the formation of secondary phases. This occurrence of secondary phases has also been documented in other metal combinations within LDH. The high concentration of hydroxide ions at pH 13 results in the formation of ZnAl-LDH mixed hydroxides, such as $Na[Al(OH)_4]$ and $Na_2[Zn(OH)_4]$ [45], [47]. Additionally, other mixed hydroxides, including $Na_2[Cu(OH)_4]$, $Cu(OH)_2$, and CuO, have been identified in the formation of CuAl-LDH at pH 10 [45], [47].

$$Mg^{2+} + 2OH^- \rightleftharpoons Mg(OH)_2 \quad (3)$$

$$5Mg(OH)_2 + 4CO_2 + H_2O \rightarrow Mg_2(CO_3)4(OH)_2.5H_2O \quad (4)$$

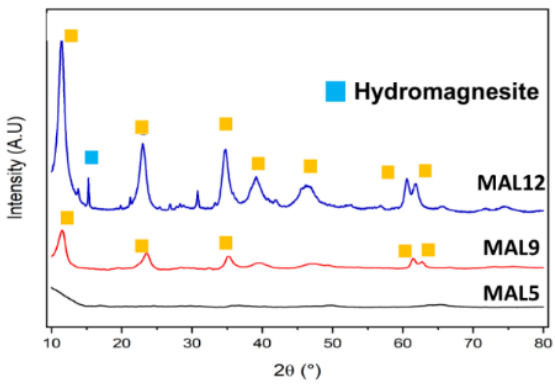

Figure 3: XRD pattern of MAL in pH of 5 (MAL5), 9 (MAL9), and 12 (MAL12).

3.3 *CIP Adsorption Performance*

3.3.1 Effect of MAL's pH synthesis

The adsorption performance of Mg/Al LDHs synthesized at different pH levels was examined, as shown in Figure 4(a). The findings reveal that the CIP adsorption capacity of MAL is influenced by the pH condition under which MAL was synthesized, reaching a peak between pH 5 and 9, before declining at pH 12. This trend is consistent with observations in other systems synthesized under similar conditions [48]. The hydrotalcite phase of the sample produced at pH 5 (MAL5) has a poorly defined structure (see Figure 2), leading to an incomplete formation of lamellar structure and basal spacing, which negatively impacts the adsorption process. As a result, MAL5 only adsorbs about 40% of CIP. In contrast, the sample synthesized at pH 9 (MAL9) shows well–defined brucite–like sheets and interlayer spaces, which facilitate effective charge balancing with CIP particles, achieving a maximum adsorption capacity of around 60%. However, although the crystal structure of the sample synthesized at pH 12 (MA12) exhibits sharp peaks indicating strong basal spacing (Figure 2), its adsorption performance plateaus compared to MAL9. This may be due to the appearance of a secondary phase, specifically hydromagnesite, which includes carbonate ions (CO_3^{2-}) in its framework, as supported by existing literature [49]. Hydromagnesite, with the formula $[4MgCO_3.Mg(OH)_2.4H_2O]$, is a common form of magnesium hydrocarbonate mineral within a layered structure [50]. Under the extreme pH conditions in MAL12, the high magnesium content leads to increased precipitation of aluminum ions as a trivalent species, while magnesium remains as a divalent ion in solution. The elevated pH also boosts the concentration of CO_3^{2-} ions from Na_2CO_3 or NaOH. This significant imbalance between the depletion of aluminum and the presence of magnesium ions encourages precipitation as hydrotalcite and the reaction with CO_3^{2-} to form hydromagnesite. Ultimately, the reduced adsorption capacity can be attributed to the formation of hydromagnesite during the synthesis of the layered double hydroxides, which decreases the availability of active surface areas [49] and limits the efficiency of CIP adsorption. In summary, MAL9 demonstrated the highest performance in CIP adsorption due to its well–defined basal spacing and pure hydrotalcite phase, making it the selected sample for further studies.

3.3.2 Adsorbent dosage

In the realm of adsorption, the ratio of adsorbent to adsorbate is crucial for achieving optimal performance. This study involved a preliminary assessment of various adsorbent doses, ranging from 0.5–2.5 mg/mL, in relation to a CIP solution with a concentration of 50 mg/L at pH 7. The adsorption capacity of MAL9 across these different doses is depicted in Figure 4(b). Starting with an initial dosage of 50.5 mg/mL, MAL9 exhibited an adsorption capacity of 62.3 mg/g. This capacity increased

significantly to 64.92 mg/g when using a dosage of 1 mg/mL. However, as the adsorbent dosage continued to rise, a gradual decline in adsorption capacity was observed. The initial increase in adsorption efficiency can be attributed to a heightened frequency of collisions between the adsorbent and adsorbate, which corresponded with a larger availability of active surface sites. In contrast, the subsequent decrease in capacity is likely due to the aggregation of adsorbent particles at higher dosages. Such aggregation can diminish the effective surface area and extend diffusion pathways, both of which negatively affect adsorption performance [21]. Additionally, higher concentrations of adsorbent can lead to the exchange of higher–energy surface sites with lower–energy fractions, further impacting overall adsorption [51]. Thus, this study suggests that an optimal dosage of 1 mg/mL of MAL9 is recommended for the adsorption of a ciprofloxacin solution at a concentration of 50 mg/L. These findings align with existing research, reinforcing the effectiveness of the identified dosage [21].

3.3.3 Effect of CIP solution pH

In practical applications, waste treatment requires a diverse range of solutions, including considerations of pH levels. One notable water pollutant is the antibiotic CIP, which is particularly persistent due to its structural changes based on the medium's pH. Studies, such as those conducted by Igwegbe *et al.*, [14], have explored the behavior of CIP using various adsorbents across different pH conditions. Figure 4c illustrates the adsorption behavior of the MAL system at various pH levels. It is evident that in low pH conditions (1–4), the adsorption capacity is minimal. However, this capacity significantly increases, reaching a seven–fold increase at pH 6. From pH 6 to 10, the adsorption level stabilizes, but at extremely alkaline conditions (pH 12), the adsorption rate drops dramatically to only 40%. This pattern is closely linked to the dynamic changes in CIP's ionic state, which affects its affinity for the MAL9 system. Key factors in the adsorption process include the pH of the solution, the point of zero charge, and the pKa values of the adsorbate. CIP has two functional groups—hydroxyl and amine—and, consequently, two pKa values: pKa_1 at 5.9 and pKa_2 at 8.89. In low pH conditions, the ionic state of CIP becomes positively charged due to the protonated amine group [10], [52]. This positive charge does not interact well with the MAL9 framework, which has a net positive charge due to the presence of divalent and trivalent metals. As reported in previous studies [53], the point of zero charge for MALranges from 7.8 to 12, leading to a repulsive interaction between CIP and MAL9. Conversely, at pH levels between 6 and 9, both the amine and hydroxyl functional groups become activated, forming a zwitterion that enhances electrostatic interactions.

Overall, the pH-dependent adsorption profile shows that MAL9 achieves its highest adsorption efficiency under mildly basic conditions. Within this pH range, ciprofloxacin predominantly exists in its zwitterionic form, enabling optimal electrostatic interactions and ion exchange with the positively charged LDH layers. This is also supported by the elevated surface area (2,671 m^2/g) and large pore volume (2.43 cm^3/g) of MAL9, as demonstrated before (Table 1), which facilitates molecular diffusion and accessibility of active sites, thereby enhancing adsorption. However, at strongly alkaline conditions (MAL12), the adsorption capacity significantly decreases. This is due to the partial conversion of the LDH surface into hydromagnesite or magnesite phase (Figure 3). As a result, the availability of reactive hydroxyl groups is reduced and chemisorptive interactions are hindered. Therefore, MAL9's superior performance can be attributed to the synergistic influence of favorable surface morphology and pore structure combined with stable surface chemistry under near–neutral pH conditions.

3.3.4 Effect of competitive anions

In the real polluted water system, CIP compounds are always in coexistence with other anions [14] as a competitive agent, hence we studied the adsorption with simulated polluted water containing several competitive ions of mono-, di-, and trivalent, which are Cl^-, CO_3^{2-}, SO_4^{2-}, and PO_4^{3-}. The influence of those interfering anions on the adsorption capacity was evaluated (Figure 4d). It is clearly shown that the percentage of CIP uptake decreases in the order $Cl^- > CO_3^{2-} > SO_4^{2-} > PO_4^{3-}$. It is noticeably implied that the competitive effect between the existing anion in the MAL9 framework with the new-former anion is greater when the given ion has a larger ionic state. The CIP uptake is insignificantly decreased between the absence and the presence of Cl^- anion, but noticeably lower in the presence of divalent and trivalent anions such as SO_4^{2-} and PO_4^{3-}.

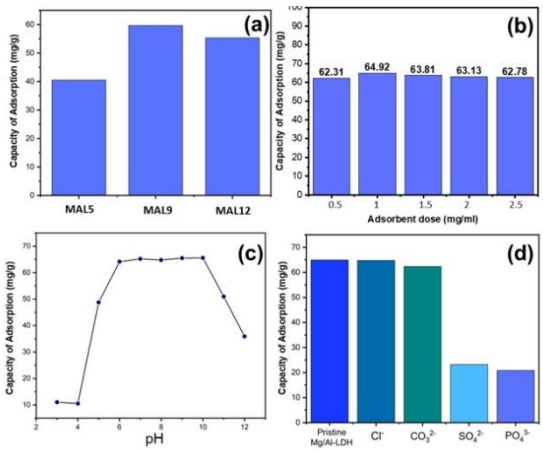

Figure 4: (a) The adsorption capacity of pH–synthesized Mg/Al LDH, (b) the amount of the adsorbent used, (c) the pH level of the CIP solution, and (d) the influence of co–ions present in the solution.

The addition of Cl^- as a monovalent anion is similar to the CIP mono–ionic state, hence the competitive effect is not deemed enough to interfere with CIP adsorption. However, the presence of sulfate and phosphate as divalent and trivalent anions will provide a higher ionic attraction with Mg^{2+} and Al^{3+} in MAL frameworks and, hence, will interfere with CIP adsorption. Novillo *et al.*, [24] show the phenomenon that LDH has a higher affinity towards divalent anions than monovalent anions, which is also in similar notes in other studies [14], [54], [55]. Additionally, the presence of carbonate ions did not significantly change the performance, while sulfate ions did, although carbonate and sulfate are at a similar level of ionic state. The plausible reason is that the intercalation layer of hydrotalcite has included the carbonate anion in the first place through Na_2CO_3/NaOH solution. Once the carbonate ion is intercalated, it resists another anion exchange, including the newcomer of carbonate anion [56].

The variation in adsorption performance among different co–ions (Figure 4d) demonstrates that the surface chemistry and interlayer anion configuration of LDH play a crucial role in controlling the adsorption process. MAL9, which contains CO_3^{2-} as the dominant interlayer anion, exhibited the highest adsorption capacity due to its optimal balance between anion exchangeability and structural stability. The carbonate species not only maintain a well–ordered layered structure but also create a favorable surface charge environment that enhances the electrostatic interaction and hydrogen bonding with ciprofloxacin molecules. In contrast, the presence of multivalent anions such as SO_4^{2-} and PO_4^{3-} reduces adsorption efficiency because these anions strongly bind to the interlayer sites, limiting the accessibility of active sites for the organic molecule. Thus, the superior performance of MAL9 can be attributed to its surface chemistry governed by interlayer carbonate ions, which promote a mixed mechanism of anion exchange and surface complexation, consistent with chemisorption–dominated adsorption [57], [58].

3.4 *Adsorption isotherm and kinetics*

The interaction between the adsorbent and adsorbate is a critical area of study for elucidating the adsorption mechanism. As illustrated in Figure 5(a), the data reveal a linear correlation between adsorbate concentration and adsorption capacity [40]. This relationship suggests that an increase in CIP concentration enhances the likelihood of effective collisions between the adsorbate molecules and the surface of the adsorbent, subsequently facilitating the mass transfer from the solution phase to the solid phase [59]. By methodically increasing the adsorbate concentration while maintaining a fixed dose of adsorbent under controlled isothermal conditions, we can gain further insights into the adsorption behavior. Understanding the adsorption equilibrium is essential for comprehensive analysis, and the isotherm provides valuable information about the interactions between the adsorbate molecules and the adsorbent surface [40]. The Freundlich and Harkin-Jura isotherm models are commonly utilized to describe these interactions [13], [60], as shown in Figure 5(a), respectively. Our regression analysis indicates that the Freundlich model ($R^2 = 0.994$) offers a superior fit compared to the Harkin-Jura model ($R^2 = 0.972$), positioning the Freundlich model as the most representative framework for analyzing the isothermal adsorption of CIP by the MAL9 system. This model suggests a spontaneous mechanism of multilayer adsorption [52], [61]. Particularly noteworthy is the parameter value of 1/n, which reflects the heterogeneity of the adsorbent surface; our findings yield a value of 0.92, indicating a high level of heterogeneity [40]. Additionally, the Freundlich model constant n, representing the adsorption intensity constant, exceeding 1 for MAL, signifies substantial adsorption affinity in MAL. Moreover, the isotherm model enables us to assess the maximum capacity of the sorption process, as

indicated by the K_f value. Our results demonstrate that the MAL9 system exhibits a maximum adsorption capacity of 95.15 mg/g at the initial concentration of CIP as much as 100 mg/L.

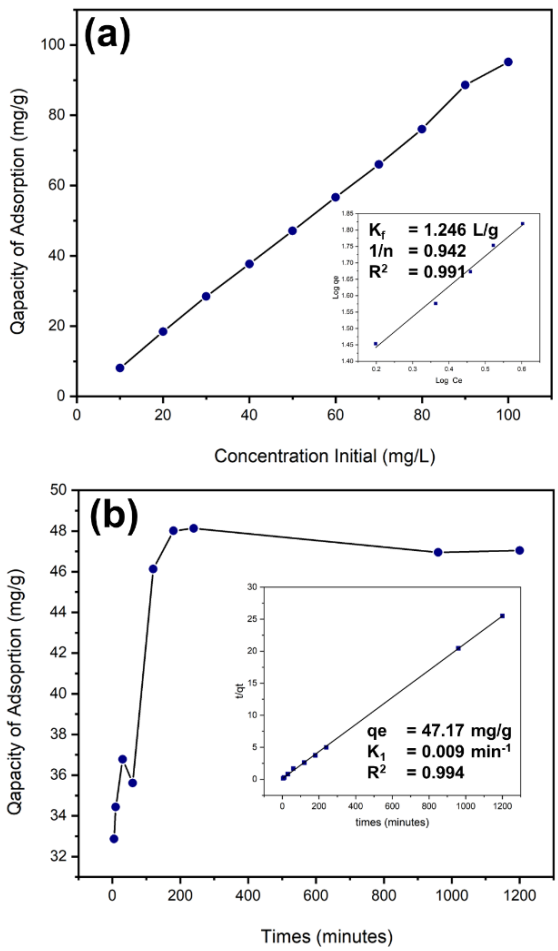

Figure 5: (a) The isothermal adsorption plot of MAL9 utilizing the Freundlich model demonstrates the variation of CIP concentration and (b) the kinetic analysis is presented through the adsorption capacity of MAL9 onto CIP over time, including a fitting of the pseudo–second–order model.

Figure 5(b) further illustrates that equilibrium is achieved within approximately 100 min, a timeframe that is notably faster compared to other corresponding LDH systems [40] This rapid uptake is primarily attributed to the substantial diffusion from the solution phase to the external solid phase, while the subsequent gradual rate of adsorption can be ascribed to internal surface retention and interaction processes [40]. Additionally, the equilibrium concentration of adsorbed CIP within the MAL9 system, shown in Table 2, is measured at 47.17 mg/g, a value that aligns well with findings from both LDH and non–LDH systems [2], [13], [49]. In exploring kinetic models, the pseudo–first order and pseudo–second order models are frequently employed in adsorption studies [14], [21], [40]. The pseudo-first order model pertains to physical adsorption, where the ratio of solute concentration to solid significantly influences the sorption rate. In contrast, the pseudo–second order model addresses the limiting factors of electron sharing between the adsorbate and adsorbent, suggesting a chemisorption process [14], [62]. Together with Table 2, our analysis identifies the pseudo–second order model as providing the highest linear regression outcomes, corroborating results reported in various adsorption systems, including Fe_3O_4–Zn–Cr LDH [14], although in several cases, mix-adsorption with physisorption is also plausible [63]–[65].

Table 2: Isotherm and kinetics parameters of CIP adsorption onto MAL9.

Freundlich isotherm	***K_f (L/g)***	**1/n**	**R^2**
	1.246	0.942	0.99
Pseudo-second order	**q_e, calculated (mg g^{-1})**	**K_1 min^{-1}**	**R^2**
	47.17	0.009	0.99

3.5 *Materials reusability*

High regeneration properties are integral to enhancing the effectiveness of adsorption applications, particularly for waste material management. This study explores the adsorption–desorption process over four cycles, utilizing an eluent derived from an acidic solution (CH_3COOH) to facilitate the removal of adsorbates from the surface sites of the adsorbent. The presence of hydrogen ions (H^+) promotes the attachment of the CIP molecule through dipole–dipole and electrostatic interactions, thereby supporting the regeneration of the surface sites. Although it is not dominant, the supporting involvement of physisorption where a weak intermolecular interaction could help regeneration of the adsorption capacity up to 80–90% in the 4th cycle, which underlines the presence of mix-adosorption mechanism [66]. The observed adsorption capacity of the MAL9 material for the CIP solution, as illustrated in Figure 6,

demonstrates a consistent decline over successive cycles, recorded at 49.42, 35.07, 14.15, and 10.27 mg/g, respectively. This trend coincides with a gradual decrease in the concentration of CIP removed from the solution, indicating a performance reduction of approximately 25.67% per cycle. This decrease in efficiency may be attributed to the limitations of the eluent, as CH_3COOH likely solubilizes only a partial fraction of the CIP present within the MAL9 system, resulting in the occupation of some surface sites and consequently impairing adsorption performance. Additionally, potential leaching of fractions from the surface sites, due to the dissolution of Mg^{2+} and Al^{3+} ions in the acid medium [67], thereby supporting the regeneration of the surface sites.

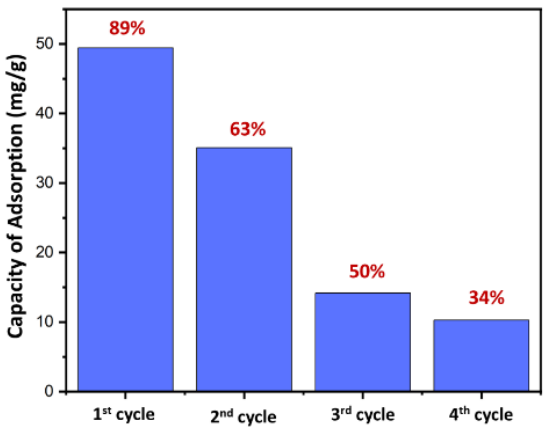

Figure 6: Adsorption capacity of MAL9 in several applied cycles.

As anticipated, the reusability of this system may be less than that of more complex hierarchical structures based on layered double hydroxides (LDH), which typically display a greater variety of metal combinations and structural frameworks [39], [40], [68]. However, the three-dimensional frameworks examined herein not only offer tunable morphology but also preserve their layered integrity during the adsorption–desorption process, thereby enhancing performance over multiple applications. For instance, CaMgAl-LDH has been reported to achieve a CIP retention rate exceeding 62% after six cycles [69], while the three–dimensional flower–like hollow structure of CoAl-LDH retains over 75% of CIP after five cycles [40]. Furthermore, a three–dimensional zeolite ZIF–67 supporting CuCo-LDH has demonstrated an adsorption performance of up to 70% in the removal of methylene orange (MO) [39]. For example, fine–layered structures such as SiO–coated MgAl-LDH exhibit a retention rate of below 10% for anionic pollutants after three cycles [70], and layered Ni/Al-LDH show a retention rate below 35% for methylene blue over the same number of cycles [71]. Given this comparable performance at an initial stage of the LDH framework's development, there is considerable potential for advancing adsorption efficiency through the exploration of more complex frameworks in future research endeavors.

3.6 *After adsorption*

The charge–balancing mechanisms within their structure significantly influence the adsorption performance of LDH. The removal of pollutants from aqueous solutions necessitates multiple interactions between the adsorbate and the surface sites of the adsorbent, including the involvement of functional groups. Additionally, these interactions are enhanced by the presence of interlayer anions and the adsorbent's high surface area and porosity. Therefore, examining the structural properties of LDH both before and after treatment is critical for assessing their effectiveness.

In the context of CIP, as the adsorbate interacts with Mg/Al LDH, various interactions are engaged. As illustrated in Figure 7a, there is no notable shift in the three main characteristic peaks of MAL9, indicating a well–preserved structure throughout the sorption process. The presence of CIP is confirmed by the sharp peak observed at $2\theta = 20°–40°$, which reflects the crystal phase of the compound. Furthermore, while previous studies often report deviations in the lattice structure of adsorbents following treatment, Figure 1c reveals no additional or shifted peaks, suggesting that the crystal structure of LDH remains stable. This finding is further supported by FTIR analysis, as shown in Figure 7(b), which displays several peaks at 439, 452, 471, and 665 cm^{-1} corresponding to M–O–M vibrations and M–O–H bending [40], [72]. The sharp peak at 1355 cm^{-1} indicates the asymmetric stretching of carbonate anions [73] or intercalated NO_3^- [24], while the peak at 1633 cm^{-1} corresponds to interlayer water bending vibrations [74]. Notably, the vibration at 3360 cm^{-1} is associated with the –OH stretching of water molecules in the brucite layer [73]. A significant observation is the presence of an additional peak around 1640–1570 cm^{-1}, which is indicative of the characteristic stretching mode of the carboxyl group in the carbonate ion derived from the presence of CIP [2], [10].

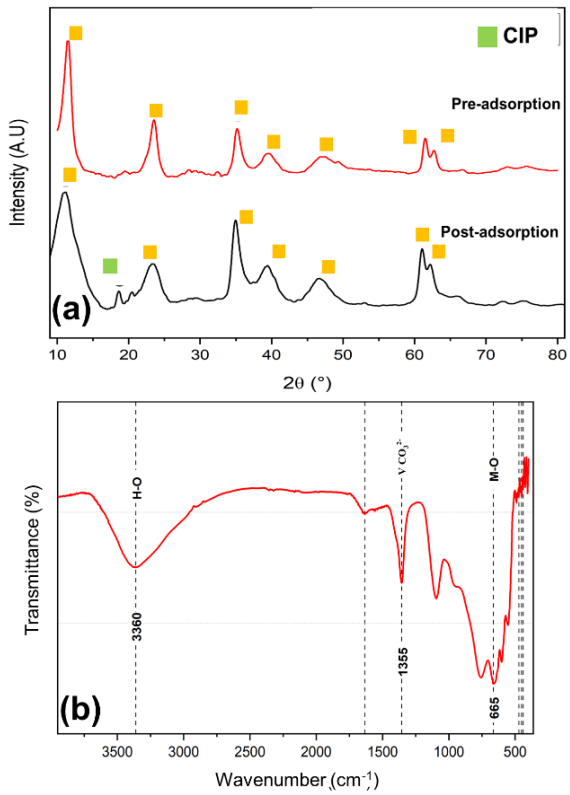

Figure 7: (a) XRD patterns of the MAL9 system, illustrating the data both before and after the adsorption of CIP. Additionally, (b) the FTIR spectrum of MAL9 following the adsorption process.

While the crystal lattice structure exhibits no significant deviations, the morphological analysis following the adsorption process shows clear changes (Figure 8). Compared to Figure 1(b)–(c), the MAL system depicted in Figure 8(a)–(b) appears rougher and larger, which can be attributed to the incorporation of CIP within the LDH microstructure. Furthermore, a comparative analysis underscores these differences; Figure 8(a) and (b) present blurring and deviations in the layered structure of the MAL system when juxtaposed with Figure 1(c). These visual alterations reinforce the successful integration of the MAL system and highlight the efficacy of the adsorption process.

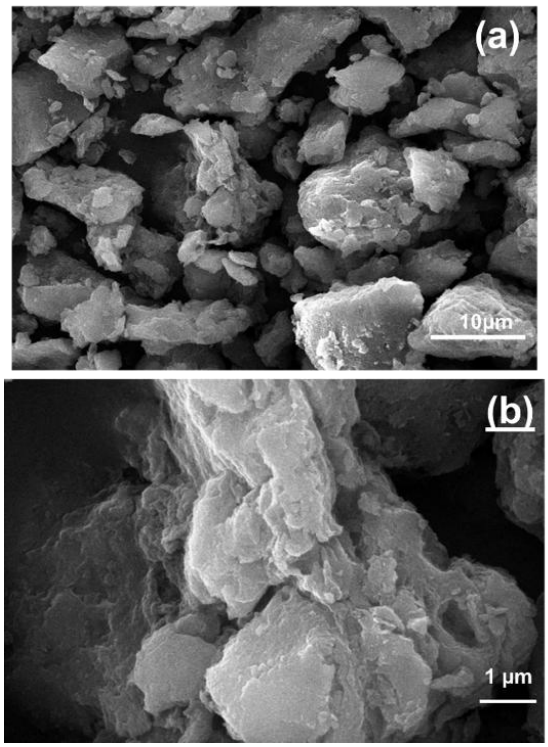

Figure 8: SEM images showcase the fractured surface of MALat magnifications of (a) 2500x and (b) 10000x, respectively, following the sorption process.

3.7 *Potential of practical application*

The simple synthesis of the MgAl-LDH system in this work proposes bittern as a magnesium source with comparable yield and adsorption capacity to other magnesium source–based LDH systems. The high abundance of bittern as a salt plant by–product will bridge the gap between bulk adsorption needs and industrial benefits. Battaglia *et al.*, [75] reported a successful pilot–scale Mg^{2+} recovery plant that achieved 99% conversion of native bittern to $Mg(OH)_2$ powder from one of the bitterns of an Italian district salt plant. Although LDH–based adsorption has been frequently demonstrated in many real–world wastewater treatments, such as treating pyrophosphate (PP) in real electroplating wastewater Fu *et al.*, or removing metals and dyes from textile wastewater [76], the performance of bittern-derived LDH has begun to demonstrate feasibility in real–world treatments. Ayoub *et al.*, reported a 56% arsenic removal from native tannery wastewater via active adsorption of bittern/lime. Similarly, the use of bittern coagulant has been shown to successfully remove

>90% of the metal pollutants from batik industrial wastewater [77].

Indeed, wastewater treatment (reusing waste and converting it into valuable products to address other waste issues) is quite costly, both financially and in terms of efficiency. Widodo *et al.*, [78] successfully demonstrated the profitability and environmental benefits of a bittern recovery facility through mixed integer nonlinear modeling, which considers bittern supply, demand structure, and recovery constraints. This model presents parameters that maximize the trade–off between waste transportation costs, recovery, station investment, sales value, and environmental sustainability. The results show that total profit and environmental benefit parameters will theoretically increase in an exponential way, with increasing bittern stock, even for a decentralized scenario (small, distributed bittern recovery plants operating in parallel), which is generally assumed to be a non–profit scenario. The point of unrealistic environmental benefits, where the profit feedback does not meet the environmental feedback, is reached when bittern supply reaches 1.25–2 million tons/year, which is quite manageable given the plant's potential for expansion. The consistent success of conventional LDH and bittern derivatives in real wastewater applications, combined with proven economic feasibility and performance at pilot scale, positions the idea of bittern-LDH as a waste–to–waste solution to become more measurable.

4 Conclusions

The study successfully synthesized and characterized Mg/Al LDHs using bittern at a pH of 9, confirming the formation of a lamellar hydrotalcite-like material with well-defined basal spacing and plate-like morphology. This novel approach of using bittern as Mg^{2+} precursor realizes the concept of zero waste and gives the added value as precursors for functional nanomaterials. The MAL9 material exhibited the highest specific surface area and pore volume among the samples, contributing to its superior adsorption capacity for CIP. The study demonstrated that pH significantly influences the synthesis process, with pH 9 yielding the most optimal material. Additionally, the effect of adsorbent dosage, solution pH, time and CIP initial concentration and competitive anions on CIP adsorption was systematically investigated, revealing that the MAL9 system performed best under specific conditions. The CIP adsorption tendency on MAL9 is well- matched with the electrostatic charge between CIP and MAL 9. The electrostatic interaction is strongly involved in the CIP adsorption reaction of MAL 9. The adsorption process was best described by the pseudo-second-order kinetic model, indicating chemisorption as the dominant mechanism. At a constant pH 7, the MAL 9 shows 95.5 mg/g at a CIP initial concentration of 100 mg/L without precipitation reaction, and it is well-fitted with the Freundlich isotherm model, which means that heterogeneity in the CIP adsorption reaction. Overall, the findings provide valuable insights into the synthesis, characterization, and adsorption performance of Mg/Al LDHs, contributing to the advancement of wastewater treatment technologies.

Acknowledgment

The authors are grateful to L'orèal For Women in Science National Fellowship 2019, Research Organization of Nanotechnology and Materials and Research Organization of Life Science and Environment for the research funding. Also for the Research Center for Environmental and Clean Technology - BRIN and Nano Center Indonesia for providing the research facilities.

Author Contributions

S.P.: Conceptualization, Formal analysis, Methodology, Supervision, Validation, Writing – review & editing; R.A.: Formal analysis, Validation, Visualization, Writing – original draft; S.A.L.: Investigation, Formal analysis; F.D.: Formal analysis; A.Z.M.: Formal analysis, Resources, Writing – review & editing; M.N.: Resources, Writing – review & editing; A.N.: Formal analysis, Writing – review & editing.

Conflicts of Interest

The authors declare that they have no known competing financial interests or personal relationships that could have appeared to influence the work reported in this paper.

Declaration of generative AI and AI-assisted technologies in the writing process

The authors utilized the ChatGPT tool to enhance the language and readability of the manuscript.

References

[1] A. L. Johnston, E. Lester, O. Williams, and R. L. Gomes, "Understanding layered double hydroxide properties as sorbent materials for removing organic pollutants from environmental waters," *Journal of Environmental Chemical Engineering*, vol. 9, no. 4, 2021, Art. no. 105197, doi: 10.1016/j.jece.2021.105197.

[2] W. K. Wakejo, B. T. Meshasha, J. W. Kang, and Y. Chebude, "Enhanced ciprofloxacin removal from aqueous solution using a chemically modified biochar derived from Bamboo Sawdust: Adsorption process optimization with response surface methodology," *Adsorption Science and Technology*, vol. 2022, 2022, doi: 10.1155/2022/2699530.

[3] C. A. Igwegbe, S. N. Oba, C. O. Aniagor, A. G. Adeniyi, and J. O. Ighalo, "Adsorption of ciprofloxacin from water: A comprehensive review," *Journal of Industrial and Engineering Chemistry*, vol. 93, pp. 57–77, 2021, doi: 10.1016/j.jiec.2020.09.023.

[4] Z. Movasaghi, B. Yan, and C. Niu, "Adsorption of ciprofloxacin from water by pretreated oat hulls: Equilibrium, kinetic, and thermodynamic studies," *Industrial Crops and Products*, vol. 127, pp. 237–250, 2019, doi: 10.1016/j.indcrop.2018.10.051.

[5] M. Sagaseta de Ilurdoz, J. J. Sadhwani, and J. V. Reboso, "Antibiotic removal processes from water & wastewater for the protection of the aquatic environment - A review," *Journal of Water Process Engineering*, vol. 45, 2022, Art. no. 102474, doi: 10.1016/j.jwpe.2021.102474.

[6] O. Falyouna, I. Maamoun, K. Bensaida, A. Tahara, Y. Sugihara, and O. Eljamal, "Encapsulation of iron nanoparticles with magnesium hydroxide shell for remarkable removal of ciprofloxacin from contaminated water," *Journal of Colloid and Interface Science*, vol. 605, pp. 813–827, Jan. 2022, doi: 10.1016/j.jcis.2021.07.154.

[7] D. Balarak and G. McKay, "Utilization of MWCNTs/Al $_2O_3$ as adsorbent for ciprofloxacin removal: Equilibrium, kinetics and thermodynamic studies," *Journal of Environmental Science and Health, Part A*, vol. 56, no. 3, pp. 324–333, Feb. 2021, doi: 10.1080/10934529.2021.1873674.

[8] C. Liang, X. Zhang, P. Feng, H. Chai, and Y. Huang, "ZIF-67 derived hollow cobalt sulfide as superior adsorbent for effective adsorption removal of ciprofloxacin antibiotics," *Chemical Engineering Journal*, vol. 344, pp. 95–104, 2018, doi: 10.1016/j.cej.2018.03.064.

[9] T. Atugoda, C. Gunawardane, M. Ahmad, and M. Vithanage, "Mechanistic interaction of ciprofloxacin on zeolite modified seaweed (Sargassum crassifolium) derived biochar: Kinetics, isotherm and thermodynamics," *Chemosphere*, vol. 281, 2021, Art. no. 130676, doi: 10.1016/j.chemosphere.2021.130676.

[10] Z. Movasaghi, B. Yan, and C. Niu, "Adsorption of ciprofloxacin from water by pretreated oat hulls: Equilibrium, kinetic, and thermodynamic studies," *Industrial Crops and Productions*, vol. 127, pp. 237–250, 2019, doi: 10.1016/j.indcrop.2018.10.051.

[11] Z. Zhao, J. Zhao, and C. Yang, "Efficient removal of ciprofloxacin by peroxymonosulfate/Mn_3O_4-MnO_2 catalytic oxidation system," *Chemical Engineering Journal*, vol. 327, pp. 481–489, Nov. 2017, doi: 10.1016/j.cej.2017.06.064.

[12] B. De Witte, J. Dewulf, K. Demeestere, and H. Van Langenhove, "Ozonation and advanced oxidation by the peroxone process of ciprofloxacin in water," *Journal of Hazardous Materials*, vol. 161, no. 2–3, pp. 701–708, Jan. 2009, doi: 10.1016/j.jhazmat.2008.04.021.

[13] C. Liang, X. Zhang, P. Feng, H. Chai, and Y. Huang, "ZIF-67 derived hollow cobalt sulfide as superior adsorbent for effective adsorption removal of ciprofloxacin antibiotics," *Chemical Engineering Journal*, vol. 344, no. January, pp. 95–104, 2018, doi: 10.1016/j.cej.2018.03.064.

[14] C. A. Igwegbe, S. N. Oba, C. O. Aniagor, A. G. Adeniyi, and J. O. Ighalo, "Adsorption of ciprofloxacin from water: A comprehensive review," *Journal of Industrial and Engineering Chemistry*, vol. 93, pp. 57–77, 2021, doi: 10.1016/j.jiec.2020.09.023.

[15] A. Cuprys et al., "Insights into the Simultaneous Sorption of Ciprofloxacin and Heavy Metals Using Functionalized Biochar," *Water (Basel)*, vol. 13, no. 19, p. 2768, Oct. 2021, doi: 10.3390/w13192768.

[16] L. Qalyoubi, A. Al-Othman, S. Al-Asheh, K. Shirvanimoghaddam, R. Mahmoodi, and M. Naebe, "Textile-based biochar for the removal of ciprofloxacin antibiotics from water," *Emergent Materials*, Jun. 2023, doi: 10.1007/s42247-023-00512-0.

[17] X. Peng, F. Hu, T. Zhang, F. Qiu, and H. Dai, "Amine-functionalized magnetic bamboo-based activated carbon adsorptive removal of ciprofloxacin and norfloxacin: A batch and fixed-bed column study," *Bioresources Technologies*, vol. 249, pp. 924–934, 2018, doi: 10.1016/j.biortech.2017.10.095.

[18] H. Gao *et al.*, "Surface Area- and Structure-Dependent Effects of LDH for Highly Efficient Dye Removal," *ACS Sustainable Chemistry Engineering*, vol. 7, no. 1, pp. 905–915, 2019, doi: 10.1021/acssuschemeng.8b04476.

[19] Z. Yang *et al.*, "Utilization of LDH-based materials as potential adsorbents and photocatalysts for the decontamination of dyes wastewater: A review," *RSC Advances*, vol. 6, no. 83, pp. 79415–79436, 2016, doi: 10.1039/c6ra12727d.

[20] T. T. H. Nguyen, X. T. T. Nguyen, C. Q. Nguyen, and P. H. Tran, "Porous metal oxides derived from Cu–Al layered double hydroxide as an efficient heterogeneous catalyst for the Friedel–Crafts alkylation of indoles with benzaldehydes under microwave irradiation," *Heliyon*, vol. 4, no. 11, p. e00966, 2018, doi: 10.1016/j.heliyon.2018.e00966.

[21] Z. Yang *et al.*, "Utilization of LDH-based materials as potential adsorbents and photocatalysts for the decontamination of dyes wastewater: A review," *RSC Advances*, vol. 6, no. 83, pp. 79415–79436, 2016, doi: 10.1039/c6ra12727d.

[22] C. Novillo, D. Guaya, A. Allen-Perkins Avendaño, C. Armijos, J. L. Cortina, and I. Cota, "Evaluation of phosphate removal capacity of Mg/Al layered double hydroxides from aqueous solutions," *Fuel*, vol. 138, no. June 2017, pp. 72–79, 2014, doi: 10.1016/j.fuel.2014.07.010.

[23] T. T. H. Nguyen, X. T. T. Nguyen, C. Q. Nguyen, and P. H. Tran, "Porous metal oxides derived from Cu–Al layered double hydroxide as an efficient heterogeneous catalyst for the Friedel–Crafts alkylation of indoles with benzaldehydes under microwave irradiation," *Heliyon*, vol. 4, no. 11, p. e00966, 2018, doi: 10.1016/j.heliyon.2018.e00966.

[24] C. Novillo, D. Guaya, A. Allen-Perkins Avendaño, C. Armijos, J. L. Cortina, and I. Cota, "Evaluation of phosphate removal capacity of Mg/Al layered double hydroxides from aqueous solutions," *Fuel*, vol. 138, no. June 2017, pp. 72–79, 2014, doi: 10.1016/j.fuel.2014.07.010.

[25] T. Hibino, "Anion Selectivity of Layered Double Hydroxides: Effects of Crystallinity and Charge Density," *European Journal of Inorganic Chemistry*, vol. 2018, no. 6, pp. 722–730, 2018, doi: 10.1002/ejic.201701067.

[26] S. Miyata, "Anion-Exchange properties of hydrotalcite-like compounds," *Clays and Clay Minerals*, vol. 31, no. 4, pp. 305–311, 1983, doi: 10.1346/CCMN.1983.0310409.

[27] S. Saha, S. Ray, R. Acharya, T. K. Chatterjee, and J. Chakraborty, "Magnesium, zinc and calcium aluminium layered double hydroxide-drug nanohybrids: A comprehensive study," *Applied Clay Science*, vol. 135, pp. 493–509, 2017, doi: 10.1016/j.clay.2016.09.030.

[28] S. Naseem, B. Gevers, R. Boldt, F. J. W. J. Labuschagné, and A. Leuteritz, "Comparison of transition metal (Fe, Co, Ni, Cu, and Zn) containing tri-metal layered double hydroxides (LDHs) prepared by urea hydrolysis," *RSC Advances*, vol. 9, no. 6, pp. 3030–3040, 2019, doi: 10.1039/c8ra10165e.

[29] K. Nejati, H. Keypour, P. D. K. Nezhad, Z. Rezvani, and K. Asadpour-Zeynali, "Preparation and characterization of cetirizine intercalated layered double hydroxide and chitosan nanocomposites," *Journal of the Taiwan Institute of Chemical Engineers*, vol. 53, pp. 168–175, 2015, doi: 10.1016/j.jtice.2015.02.035.

[30] R. G. L. Gonçalves et al., "Performance of magnetite/ layered double hydroxide composite for dye removal via adsorption, Fenton and photo-Fenton processes," *Applied Clay Science*, vol. 179, p. 105152, 2019, doi: 10.1016/j.clay.2019.105152.

[31] N. Baliarsingh, K. M. Parida, and G. C. Pradhan, "Effects of Co, Ni, Cu, and Zn on photophysical and photocatalytic properties of carbonate intercalated MII/Cr LDHs for enhanced photodegradation of methyl orange," *Industrial and Engineering Chemistry Research*, vol. 53, no. 10, pp. 3834–3841, Mar. 2014, doi: 10.1021/ie403769b.

[32] M. Del Arco, M. V. G. Galiano, V. Rives, R. Trujillano, and P. Malet, "Preparation and study of decavanadate-pillared hydrotalcite-like anionic clays containing cobalt and chromium,"

Inorganic Chemistry, vol. 35, no. 22, pp. 6362–6372, 1996, doi: 10.1021/ic9601551.

[33] R. G. L. Gonçalves et al., "Performance of magnetite/ layered double hydroxide composite for dye removal via adsorption, Fenton and photo-Fenton processes," *Applied Clay Science*, vol. 179, p. 105152, 2019, doi: 10.1016/j.clay.2019.105152.

[34] Z. P. Xu, G. S. Stevenson, C.-Q. Lu, G. Q. (Max) Lu, P. F. Bartlett, and P. P. Gray, "Stable suspension of layered double hydroxide nanoparticles in aqueous solution," *Journal of the American Chemical Society*, vol. 128, no. 1, pp. 36–37, Jan. 2006, doi: 10.1021/ja056652a.

[35] S. Saha, S. Ray, R. Acharya, T. K. Chatterjee, and J. Chakraborty, "Magnesium, zinc and calcium aluminium layered double hydroxide-drug nanohybrids: A comprehensive study," *Applied Clay Science*, vol. 135, pp. 493–509, 2017, doi: 10.1016/j.clay.2016.09.030.

[36] T. Hibino, "Anion selectivity of layered double hydroxides: Effects of crystallinity and charge density," *European Journal of Inorganic Chemistry*, vol. 2018, no. 6, pp. 722–730, 2018, doi: 10.1002/ejic.201701067.

[37] A. R. Auxilio et al., "Adsorption and intercalation of acid blue 9 on Mg-Al layered double hydroxides of variable metal composition," *Polyhedron*, vol. 26, no. 14, pp. 3479–3490, 2007, doi: 10.1016/j.poly.2007.03.019.

[38] S. Saghir and Z. Xiao, "Hierarchical mesoporous ZIF-67@LDH for efficient adsorption of aqueous methyl orange and alizarine red s.," *Powder Technology*, vol. 377, pp. 453–463, 2021, doi: 10.1016/j.powtec.2020.09.006.

[39] S. Saghir and Z. Xiao, "Hierarchical mesoporous ZIF-67@LDH for efficient adsorption of aqueous methyl orange and alizarine red s.," *Powder Technology*, vol. 377, pp. 453–463, 2021, doi: 10.1016/j.powtec.2020.09.006.

[40] H. Gao et al., "Surface area- and structure-dependent effects of LDH for highly efficient dye removal," *ACS Sustainable Chemistry and Engineering*, vol. 7, no. 1, pp. 905–915, 2019, doi: 10.1021/acssuschemeng.8b04476.

[41] A. Seron and F. Delorme, "Synthesis of layered double hydroxides (LDHs) with varying pH : A valuable contribution to the study of Mg/Al LDH formation mechanism," *Journal of Physics and Chemistry of Solids*, vol. 69, no. 5–6, pp. 1088–1090, 2008, doi: 10.1016/j.jpcs.2007.10.054.

[42] A. A. Sertsova, E. N. Subcheva, and E. V Yurtov, "Synthesis and study of structure formation of layered double hydroxides based on Mg, Zn, Cu, and Al," *Russian Journal of Inorganic Chemistry*, vol. 60, no. 1, pp. 23–32, 2015, doi: 10.1134/S0036023615010167.

[43] K. Abderrazek and E. S. Najoua Frini Srasra, "Synthesis and characterization of [Zn-Al] layered double hydroxides: Effect of the operating parameters," *Journal of the Chinese Chemical Society*, vol. 64, no. 3, pp. 346–353, 2017, doi: 10.1002/jccs.201600258.

[44] J. Liu, X. Huang, Y. Li, K.M. Sulieman, X. He and F. Sun, "Facile and large scale production of ZnO/Zn-Al layered doubled hydroxide hierarchical heterostructures," *The Journal of Physical Chemistry B*, vol. 110, no. 43, pp. 21965–21872, 2006, doi:10.1021/jp064487v.

[45] M. V Bukhtiyarova, "A review on effect of synthesis conditions on the formation of layered double hydroxides," *Journal of Solid State Chemistry*, vol. 269, pp. 494–506, 2019, doi: 10.1016/j.jssc.2018.10.018.

[46] A. Seron and F. Delorme, "Synthesis of layered double hydroxides (LDHs) with varying pH : A valuable contribution to the study of Mg/Al LDH formation mechanism," *Journal of Physics and Chemistry of Solids*, vol. 69, no. 5–6, pp. 1088–1090, 2008, doi: 10.1016/j.jpcs.2007.10.054.

[47] A. A. Sertsova, E. N. Subcheva, and E. V Yurtov, "Synthesis and study of structure formation of layered double hydroxides based on Mg, Zn, Cu, and Al," *Russian Journal of Inorganic Chemistry*, vol. 60, no. 1, pp. 23–32, 2015, doi: 10.1134/S0036023615010167.

[48] D. Zheng et al., "Parallel adsorption of low concentrated ciprofloxacin by a CoFe-LDH modified sludge biochar," *Journal of Environmental Chemical Engineering*, vol. 10, no. 5, 2022, Art. no. 108381, doi: 10.1016/j.jece.2022.108381.

[49] A. R. Auxilio et al., "Adsorption and intercalation of Acid Blue 9 on Mg-Al layered double hydroxides of variable metal composition," *Polyhedron*, vol. 26, no. 14, pp. 3479–3490, 2007, doi: 10.1016/j.poly.2007.03.019.

[50] M. Dan, J. Labuschagne, W. Focke, and I. Van Der Westhuizen, "The effect of magnesium hydroxide, hydromagnesite and layered double hydroxide on the heat stability and fire performance of plasticized poly (vinyl chloride)," *Journal of Fire Science*, vol. 33, no. 6, pp. 493–510, 2015, doi: 10.1177/0734904115612501.

[51] H. B. Zaghouane, M. Boutahala, and L. Arab, "Removal of methyl orange from aqueous solution by uncalcined and calcined MgNiAl layered double hydroxides (LDHs)," *Chemical Engineering Journal*, vol. 187, pp. 142–149, Apr. 2012, doi: 10.1016/j.cej.2012.01.112.

[52] T. Atugoda, C. Gunawardane, M. Ahmad, and M. Vithanage, "Mechanistic interaction of ciprofloxacin on zeolite modified seaweed (Sargassum crassifolium) derived biochar: Kinetics, isotherm and thermodynamics," *Chemosphere*, vol. 281, 2021, Art. no. 130676, doi: 10.1016/j.chemosphere.2021.130676.

[53] Y. Azimzadeh, N. Najafi, A. Reyhanitabar, and S. Qustan, "Modeling of phosphate removal by Mg-Al layered double hydroxide functionalized biochar and hydrochar from aqueous solutions," *Iranian Journal of Chemisry & Chemical Engineering*, vol. 40, no. 2, pp. 565–579, 2021, doi: 10.30492/ijcce.2020.38042.

[54] P. Koilraj and K. Sasaki, "Selective removal of phosphate using La-porous carbon composites from aqueous solutions: Batch and column studies," *Chemical Engineering Journal*, vol. 317, pp. 1059–1068, 2017, doi: 10.1016/j.cej.2017.02.075.

[55] M. Dan, J. Labuschagne, W. Focke, and I. Van Der Westhuizen, "The effect of magnesium hydroxide, hydromagnesite and layered double hydroxide on the heat stability and fire performance of plasticized poly (vinyl chloride)," *Journal of Fire Science*, vol. 33, no. 6, pp. 493–510, 2015, doi: 10.1177/0734904115612501.

[56] S. H. J. Eiby et al., "Competition between chloride and sulphate during the reformation of calcined hydrotalcite," *Applied Clay Science*, vol. 132–133, pp. 650–659, 2016, doi: 10.1016/j.clay.2016.08.017.

[57] A. L. Johnston, E. Lester, O. Williams, and R. L. Gomes, "Understanding Layered Double Hydroxide properties as sorbent materials for removing organic pollutants from environmental waters," *Journal of Environmental Chemistry Engineering*, vol. 9, no. 4, 2021, Art. no. 105197, doi: 10.1016/j.jece.2021.105197.

[58] C. A. Igwegbe, S. N. Oba, C. O. Aniagor, A. G. Adeniyi, and J. O. Ighalo, "Adsorption of ciprofloxacin from water: A comprehensive review," *Journal of Industrial and Engineering Chemistry*, vol. 93, pp. 57–77, Jan. 2021, doi: 10.1016/j.jiec.2020.09.023.

[59] V. J. Inglezakis, M. Balsamo, and F. Montagnaro, "Liquid-solid mass transfer in adsorption systems - An overlooked resistance?," *Industrial and Engineering Chemistry Research Journal*, vol. 59, no. 50, pp. 22007–22016, 2020, doi: 10.1021/acs.iecr.0c05032.

[60] F. Gimbert, N. Morin-Crini, F. Renault, P. M. Badot, and G. Crini, "Adsorption isotherm models for dye removal by cationized starch-based material in a single component system: Error analysis," *Journal of Hazardouz Materials*, vol. 157, no. 1, pp. 34–46, 2008, doi: 10.1016/j.jhazmat.2007.12.072.

[61] S. S. Mayakaduwa et al., "Equilibrium and kinetic mechanisms of woody biochar on aqueous glyphosate removal," *Chemosphere*, vol. 144, pp. 2516–2521, Feb. 2016, doi: 10.1016/j.chemosphere.2015.07.080.

[62] A. L. Johnston, E. Lester, O. Williams, and R. L. Gomes, "Understanding Layered Double Hydroxide properties as sorbent materials for removing organic pollutants from environmental waters," *Journal of Environmental Chemistry Engineering*, vol. 9, no. 4, p. 105197, 2021, doi: 10.1016/j.jece.2021.105197.

[63] A. R. Auxilio et al., "Adsorption and intercalation of Acid Blue 9 on Mg-Al layered double hydroxides of variable metal composition," *Polyhedron*, vol. 26, no. 14, pp. 3479–3490, 2007, doi: 10.1016/j.poly.2007.03.019.

[64] A. E. Johnston and P. R. Poulton, "Phosphorus in agriculture: A review of results from 175 years of research at rothamsted, UK," 2019, doi: 10.2134/jeq2019.02.0078.

[65] S. F. Al-Furhud et al., "Adsorption of light green dye using Mg–Al-layered double hydroxides (LDHs) with carbonate and nitrate anions," *International Journal of Environmental Science and Technology*, vol. 22, no. 14, pp. 14015–14032, Oct. 2025, doi: 10.1007/s13762-025-06494-2.

[66] M. Daud et al., "A review on the recent advances, challenges and future aspect of layered double hydroxides (LDH) – containing hybrids as promising adsorbents for dyes removal," *Journal of Molecular Liquids*, vol. 288, May 2019, Art. no. 110989, doi: 10.1016/j.molliq.2019.110989.

[67] Y. You, H. Zhao, and G. F. Vance, "Adsorption of dicamba (3,6-dichloro-2-methoxy benzoic

acid) in aqueous solution by calcined–layered double hydroxide," *Applied Clay Sciences*, vol. 21, no. 5–6, pp. 217–226, Aug. 2002, doi: 10.1016/S0169-1317(01)00102-8.

[68] Z. Ali and A. A. Mohammed, "Enhanced adsorption of ciprofloxacin from an aqueous solution using a novel CaMgAl-layered double hydroxide/red mud composite," *Results in Engineering*, vol. 23, 2024, Art. no. 102600, doi: 10.1016/j.rineng.2024.102600.

[69] Z. Ali and A. A. Mohammed, "Enhanced adsorption of ciprofloxacin from an aqueous solution using a novel CaMgAl-layered double hydroxide/red mud composite," *Results in Engineering*, vol. 23, 2024, Art. no. 102600, doi: 10.1016/j.rineng.2024.102600.

[70] M. A. Abduarahman et al., "MgAl-layered double hydroxide-coated bio-silica as an adsorbent for anionic pollutants removal : A case study of the implementation of sustainable technologies," *International Journal of Molecular Sciences*, vol. 25, no. 21, 2024, Art. no. 11837, doi: 10.3390/ijms252111837.

[71] A. Lesbani, N. R. Palapa, R. J. Sayeri, T. Taher, and N. Hidayati, "High reusability of NiAl LDH/Biochar composite in the removal methylene blue from aqueous solution," *Indonesian Journal of Chemistry*, vol. 21, no. 2, pp. 421–434, 2021, doi: 10.22146/ijc.56955.

[72] A. Zaghloul et al., "Characterization and application of MgAl layered double hydroxide for methyl orange removal from aqueous solution," *Materials Today: Proceedings*, vol. 37, no. 3, pp. 3793–3797, 2021, doi: 10.1016/ j.matpr.2020.07.676.

[73] A. Zaghloul et al., "Characterization and application of MgAl layered double hydroxide for methyl orange removal from aqueous solution," *Materials Today: Proceedings*, vol. 37, no. 3, pp. 3793–3797, 2021, doi: 10.1016/j.matpr.2020.07.676.

[74] X. Wang et al., "Comparative study of the synergistic effect of binary and ternary LDH with intumescent flame retardant on the properties of polypropylene composites," *RSC Advances*, vol. 5, no. 96, pp. 78979–78985, 2015, doi: 10.1039/C5RA15565G.

[75] G. Battaglia et al., "Evaluation of the purity of magnesium hydroxide recovered from saltwork bitterns," *Water (Switzerland)*, vol. 15, no. 1, pp. 1–22, 2023, doi: 10.3390/w15010029.

[76] T. S. Munonde, N. Madima, R. Ratshiedana, P. N. Nomngongo, L. E. Mofokeng, and R. S. Dima, "Synergistic adsorption-photocatalytic remediation of methylene blue dye from textile industry wastewater over NiFe LDH supported on tyre-ash derived activated carbon," *Applied Surface Sciences*, vol. 679, Jan. 2025, doi: 10.1016/j.apsusc.2024.161205.

[77] G. M. Ayoub, A. Hamzeh, and L. Semerjian, "Post treatment of tannery wastewater using lime/bittern coagulation and activated carbon adsorption," *Desalination*, vol. 273, no. 2–3, pp. 359–365, Jun. 2011, doi: 10.1016/j.desal.2011. 01.045.

[78] E. Widodo et al., "Analysis of bittern recovery facility using mixed-integer nonlinear programming: Centralized, decentralized, and hybrid scenarios," *International Journal of Technology*, vol. 14, no. 3, p. 638, May 2023, doi: 10.14716/ijtech.v14i3.5437.